Achieving microstructures prone to superplastic deformation in an Al-Zn-Mg-Cu alloy by equal channel angular pressing

C.M. Cepeda-Jiménez*, J.M. García-Infanta, O.A. Ruano, F. Carreño

Department of Physical Metallurgy, CENIM-CSIC, Av. Gregorio del Amo 8, 28040 Madrid, Spain

Abstract

An Al-Zn-Mg-Cu alloy without Sc or Zr additions was subjected to overaging and processing by equal channel angular pressing, obtaining a grain size of ~160 nm and a fraction of high-angle boundaries of 56%. The high elongations attained at high strain rate (10^{-2}-10^{-3} s^{-1}) and low test temperature (250-300 ºC) are attributed to the formation of new recrystallized grains, ~500 nm in size, during heating at test temperature. The presence of equiaxed grains and texture randomization in the gauge length confirms that grain boundary sliding is the operative deformation mechanism in the mentioned range of testing conditions.

Keywords: Aluminium alloys; ECAP; Mechanical properties; Microstructure Deformation mechanisms

*Corresponding author. Tel.: +34 91 5538900 ext.217; fax: +34 91 5347425.
E-mail address: cm.cepeda@cenim.csic.es (C.M. Cepeda-Jiménez)

1. Introduction

Superplastic forming (SPF) at high strain rates or low temperatures is highly desirable in industrial fabrication [1,2].

Although ECAP may be readily utilized to achieve ultrafine grains in polycrystalline metals [3-5], the retention of these small grains at elevated temperatures requires the presence of an uniform distribution of stable precipitates to inhibit grain growth [6,7]. Accordingly, the poor stability of the microcrystalline structure of Al alloys at high temperatures may be overcome by addition of suitable alloying elements (e.g. Zr or Sc [8-10]). However, these elements increase the price of alloys.

In this work, a thermomechanical processing (TMP) based in overaging and ECAP processing is proposed to develop the microstructure required to achieve superplasticity in the Al 7075 alloy without Sc or Zr additions. The initial overaging treatment optimizes the distribution of pinning particles, hindering the migration of high-angle grain boundaries during subsequent superplastic forming.

Therefore, the main aim of our investigation was to study the deformation behaviour of the overaged and ECAPed Al 7075 alloy, to confirm the possibility of superplastic behaviour, and to analyze the microstructure evolution from the as-processed condition to that after mechanical testing to determine the operative deformation mechanisms.

2. Experimental procedure

Commercial Al 7075-T651 rolled plates 12 mm thick with a composition of 5.68Zn–2.51Mg–1.59Cu–0.19Cr (in wt.%) were used. Prior to ECAP processing, as-received Al 7075-T651 samples were subjected to overaging at 280ºC during 5h to obtain an stable microstructure, free of elements in solid solution, and to minimize dynamic processes, such as nucleation and precipitate coarsening during ECAP processing. The overaged Al 7075 alloy was named as start Al 7075-O.

ECAP billets with dimensions 70mm×10mm×10mm were processed using a sharp-cornered 90º ECAP die by route B_C, at a pressing speed of 5 mm/min. Each sample was initially pressed once at room temperature (N_p=1), and then pressed repetitively up to 8 passes at 130ºC, equivalent to an imposed strain of ε=8.

The microstructure of processed samples was analyzed by transmission electron microscopy (TEM) using a JEOL JEM 2000 FX II equipment operating at 200 kV. ECAPed samples were always examined at the middle of the ECAP flow plane in order to avoid die wall effects. Samples were ground mechanically and then polished to perforation using a twin-jet electropolishing facility with a solution of 30% nitric acid in methanol at -28 ºC and 15 V.

The grain size was measured from TEM images using the linear intercept method without discriminating between high- and low-angle boundaries using the Sigma Scan Pro software. More than 300 grains were analyzed. Grain size data fell into log-normal distributions, so the geometric mean value was chosen as a measure of the size.

The microtexture was examined with an automated crystallographic orientation mapping (ACOM) tool attached to a JEOL 3010 TEM operating at 300 kV and equipped with a LaB_6 filament. This technique consists of analyzing spot diffraction patterns [11] rather than Kikuchi lines, which are considered in the EBSD (electron backscattered diffraction) technique. For studies involving large strains, the spot patterns are preferred, because they are known to be less sensitive to the internal stresses resulting from severe plastic deformation [12].

A beam size of 15 nm was used. The diffraction patterns are collected at a rate of 30 frames per second through the frame grabber and the area of interest was typically of 300 x 300 pixels. The step size was 15 nm. The use of ACOM allows imaging of the microstructure based on orientation measurements, as well as the presentation of microtexture and grain-boundary data [13]. Color-coded grain-orientation maps were

produced by assigning data points to the same grain if neighboring lattice orientations differed by less than 1º. Thus, a low-angle grain boundary (LAB) was defined by a misorientation between adjacent grains of 1º<θ<15º, and a high-angle grain boundary (HAB) was defined by θ>15º. HABs and LABs are shown as black and white lines, respectively, on the maps. However, the fraction of high-angle boundaries (f_{HAB}) was calculated from misorientation data higher than 2º. Discrete pole figures were employed to examine the microtexture corresponding to the region investigated.

Planar dog-bone tensile samples of 10 mm×3 mm×1.5 mm gauge dimensions with a radius of 3mm were machined out of the ECAP samples parallel to the flow plane and with the tensile axis parallel to the extrusion direction. These samples were tested in tension using an universal Instron 1362 testing machine at various strain rates and temperatures, ranging between 10^{-5}-10^{-1} s^{-1} and 200-400 ºC, respectively. Some samples were pulled to failure at constant strain rate, while others were subjected to strain-rate-change tests (SRC) to determine more precisely the apparent stress exponent, n_{ap} [14]. An example of the stress–strain rate data determination by means of SRC tests is given in Fig. 1. The initial strain rate used in these tests was 10^{-1} s^{-1}. A first strain rate jump down to 3.10^{-2} s^{-1} is performed after a plastic deformation of ~15-20%. Then, the strain rate is consecutive reduced in steps, each having ε~2-4%, down to $\dot{\varepsilon}$~10^{-5} s^{-1}. Subsequently, the strain rate is increased in three additional steps up to 10^{-2} s^{-1}, as a check on the repeatability of flow stress measurements.

Finally, TEM and electron backscatter diffraction (EBSD) data were taken in the grip and gauge regions of deformed samples. EBSD maps were performed in a scanning electron microscope (SEM) JEOL JSM 6500F, with a fully automatic EBSD attachment, HKL Technology, operating at an accelerating voltage and working distance of 20 kV and 15 mm, respectively. The corresponding data processing was carried out using HKL Channel 5 software. A low angle grain boundary (LAB) was defined by a misorientation between adjacent grains of 2º<θ<15º, and a high angle grain boundary (HAB) was defined by θ>15º. HABs and LABs are shown as black and white lines respectively on the maps.

3. Results and Discussion

The as start Al 7075-O alloy microstructure consisted of large grains, 350 ± 10 μm length and 15 ± 2 μm thickness [15]. Fig. 2a shows a TEM micrograph corresponding to the ECAPed-8p-130ºC Al 7075-O sample. An average (sub)grain size of ~163 ± 5 nm was achieved after ECAP processing. The (sub)grain shape was slightly elongated in the shear direction of the last ECAP pass. In addition, it can be observed high density of precipitates (100–200 nm in diameter), randomly distributed both within the grain interiors and at the grain boundaries, which are indicated by black arrows. These

spherical precipitates ($Mg(Zn_2,AlCu)$ and $Al_{18}Mg_3Cr_2$), coarsened during overaging but remained unaffected by ECAP processing [15].

The microtexture data are presented as a crystallographic orientation map and the relating {111} pole figure in Fig. 2b. Fig. 2c shows the corresponding misorientation distribution in the form of a histogram.

The orientation map (Fig. 2b) shows that the lamellar boundaries aligned with the shear direction were predominantly high-angle in character, HABs, while transverse boundaries were mainly low angle boundaries, LABs. The fraction of HABs (f_{HAB}) was 56% as shown in Fig.2c.

The ECAPed Al 7075-O sample shows a typical FCC shear texture [16,17], with multiple orientations through the A ({111}<uvw>) and B ({hkl}<110>) fibres (Fig.2b). Thus, the as-processed microstructure with strong texture and intermediate-low f_{HAB} does not seem to be a priori very prone to superplastic behaviour.

The results of the mechanical testing are summarized in Fig. 3. The strain rate ($\dot{\varepsilon}$) was plotted logarithmically against the flow stress (σ) at temperatures in the range 200 to 400ºC (Fig. 3a). For simplicity, only two curves for the as start Al 7075-O alloy tested at 200 and 400ºC have been included. The black filled symbols correspond to the ECAPed sample, while the white open symbols correspond to the as start alloy. The results corresponding to the ECAPed material tested at 400ºC have been represented by a red filled symbol. The slope of each line delineates the apparent stress exponent, n_{ap} ($=\partial \log \dot{\varepsilon}/\partial \log \sigma$). This apparent stress exponent is influenced by microstructural changes produced during deformation. n_{ap} is plotted for each curve in Fig. 3b and values between 3.2 and 8 are obtained.

The ECAPed Al 7075-O alloy exhibits a sigmoidal relationship between $\dot{\varepsilon}$ and σ (Fig. 3a). This sigmoidal relationship has been reported for superplastic alloys [18]. Furthermore, the $\dot{\varepsilon}$-σ curves for the ECAPed sample strongly shift toward lower stress values with an increase of temperature up to 350ºC. In general, the ECAPed samples exhibit lower σ than the as start Al 7075-O alloy except at 400ºC, where the $\dot{\varepsilon}$-σ curves for both materials are very similar. This is indicative that different deformation mechanisms are operative for both materials at low test temperatures.

While the minimum value of n_{ap} for the as start material is observed for the lowest $\dot{\varepsilon}$ at the given temperatures, the minimum n_{ap} is registered at $\dot{\varepsilon}$ between 10^{-3} and 10^{-2} s^{-1} at 300 and 350 ºC (Fig. 3b) for the processed material. For the as start alloy, n_{ap} is ranged between 5 and 8, while for the ECAPed samples, n_{ap} varies in the range 3.2-8. The minimum n_{ap}~3.2 for the ECAPed sample occurs at 300ºC and 10^{-2} s^{-1}, while for the ECAPed samples tested at 400 ºC n_{ap} is higher, being ~6 at 10^{-2} s^{-1}. This increase of n_{ap} at high temperature for the ECAPed material suggests a change in deformation

mechanism from GBS to slip creep, and is consistent with the advent of grain growth [19].

It is worth noting that the only difference between the as-received material and the ECAPed Al 7075 alloy is the fine grain size of the ECAPed material. The most important change observed with increasing the number of ECAP passes during the ECAP processing was the decrease of grain size [15]. Therefore, taking into account that GBS is a grain size dependent mechanism, as it is reflected in the GBS equations [20-23], it is reasonable to assume that the grain refining produced during processing results in an increase in strain rate and a decrease in the temperature at which optimum superplasticity appears in the ECAP processed sample [24,25].

Fig. 3c shows the variation in elongation to failure, e_F, with the initial $\dot{\varepsilon}$ for the as-start and ECAPed Al 7075 alloy. A horizontal line has been traced at e_F=200% to delimit the elongation above which superplasticity is usually accepted [26,27]. The as start material exhibits elongations lower than 200% over the entire $\dot{\varepsilon}$ range considered. On the other hand, at test temperatures between 250 and 300ºC, the ECAPed Al 7075-O sample was considerably more ductile than the as start material. It should be noted that elongations higher than 200% are obtained at 250ºC, a temperature that can be considered intermediate-low for aluminium alloys. In a previous work [28] an elongation value of 190% at 200ºC and 10^{-3} s^{-1} was reported for the Al 7075 alloy processed at other ECAP conditions. However, in the current work, the ECAPed Al 7075 alloy exhibited a maximum elongation of 322% at 300ºC and $\dot{\varepsilon}=10^{-3}$ s^{-1}, being more than three times that of the as start material. This corresponds to the smallest n_{ap} value, close to 3 (Fig. 3b). It is also worth noting the value of e_F=210% at 300ºC and $\dot{\varepsilon}=10^{-2}$ s^{-1}, strain rate that can be associated with high strain rate superplasticity (HSR SP), which is defined formally as $\geq 10^{-2}$ s^{-1} [29-32]. Although at 300ºC lower n_{ap} value is obtained at 10^{-2} s^{-1} than that at 10^{-3} s^{-1} (Fig.3b), the lower ductility at 10^{-2} s^{-1} is attributed, on one hand, to the difficulty of accommodating deformation at high strain rate, and on the other hand, the slight grain coarsening produced during a long tensile test at 10^{-3} s^{-1}, which stabilizes deformation and justifies the increase in the observed n_{ap} (Fig.3b).

On the contrary, the ECAPed samples tensile tested at 350ºC showed much lower ductility, with values very similar to those for the as start Al 7075-O alloy.

Therefore, the high n_{ap} values observed together with the presence of the precipitates in the initial overaged state allow us to conclude that the rate-controlling process for the as start Al 7075-O alloy is a constant substructure slip creep mechanism according to Sherby's model [33], characterized by a stress exponent n=8. Furthermore, this mechanism is operative in the as start alloy in all the range of testing conditions (10^{-2}-10^{-3} s^{-1} and 250-300ºC) where the ECAPed alloy showed much lower n_{ap} values, associated in this work with GBS mechanism.

For the ECAPed sample, the observation of lower stresses, ductility values higher than 200% and n_{ap} decreasing towards 2 suggest a transition to a GBS mechanism [34], that should be rate controlling already at 250ºC (Fig. 3c). The ductility enhancement of the ECAPed alloy between 350 and 400ºC is lost and the flow stress at 400ºC is similar to that of the as-start material (Fig. 3a). In addition, the n_{ap} values were consistently higher than 5 for the various $\dot{\varepsilon}$, indicating again a change into a slip creep mechanism.

Several specimens were examined by TEM after tensile testing. Fig. 4 shows an example for the ECAPed sample pulled to failure at 300ºC and 10^{-2} s^{-1}, specimen that exhibited HSR SP and elongation of 210%. The average grain size in the grip section (Fig. 4a) was 0.9 ± 0.1 μm, showing a recrystallized structure, evolved during heating at the test temperature. By contrast, the average grain size in the gauge region (Fig. 4b and c at two magnifications) was measured as 500 ± 20 nm, which is significantly larger than the as-ECAPed grain size of ~160 nm (Fig. 2a). It is therefore assumed that continuous static recrystallization occurs during heating to the test temperature giving result to a grain size that is defined by the distance between precipitates. It is apparent that the precipitates that coarsened during overaging pinned the grain boundaries and prevented abnormal grain growth. However, dynamic recrystallization does not occur during superplastic deformation because neither a peak at low strains, nor stress oscillations, nor dynamic strain softening, which is typical of continuous recrystallization, are observed in the stress-strain curves [35,36]. Furthermore, as it will be seen below, a significant shift in the misorientation distribution toward random texture is obtained after deformation in the gauge length. This texture evolution is in contrast to microstructures that evolve during superplastic straining via a continuous recrystallization, where retention of prior deformation textures and gradual evolution of high-angle boundaries are observed during superplastic straining [37].

On the other hand, the grain size in the gauge region is slightly finer than in the grip region. It is our contention that during the tensile test the grain size in the grip grows more quickly than that in the gauge length where GBS is taking place. This behaviour will be discussed below.

Fig. 5 shows EBSD orientation maps and <111> pole figures for the grip (a,e,g) and gauge (b,f,h) sections of the ECAPed Al 7075-O alloy subjected to SRC tests at 300ºC (Fig. 5a,b), 350ºC (Fig. 5e,f) and 400ºC (Fig. 5g,h). It is worth noting that deformation during the SRC tests was performed mostly at 10^{-2} s^{-1} (Fig. 1), and the total time at test temperature was about 65 min, which is considerably longer than that corresponding to the samples shown in Fig. 4 (~20 min), tested at constant strain rate. Misorientation histograms corresponding to EBSD maps in Fig. 5a and b are shown in Fig. 5c and d, respectively. Fig. 5a and b corresponding to the sample tested at 300ºC shows an equiaxed (sub)grain structure both in the grip and gauge section. Due to the longer time characterizing the SRC test, the grain size observed both in the grip and gauge regions

is coarser (2 ± 0.5 μm) than that observed in the sample of Fig. 4. This grain growth observed as a function of the testing time justifies the higher n_{ap}~3 value than the theoretical n=2 during superplastic deformation, as predicted by GBS equations [20-23].

The undeformed grip region (Fig. 5a) shows a slight increase in shear texture intensity respect to the as-processed sample (Fig. 2b) and no new texture components are apparent. The texture retention and the development of a bimodal grain boundary misorientation distribution at 300ºC, as shown in Fig. 5c, are consistent with the occurrence of static recovery and continuous recrystallization [38]. On the other hand, there is a significant shift in the misorientation distribution toward random after deformation at 300ºC (Fig. 5d), being very close to the random grain assembly predicted by Mackenzie [39], with f_{HAB}~83%. The reduction in texture intensity and the evidence of fairly equiaxed grains after tensile testing, without visible elongation along the tensile axis (Fig. 5b), is indicative of a GBS mechanism which implies multiple grain rotation [40] and absence of dislocation movement that would involve a reinforcement of certain texture components [41,42]. In addition, as demonstrated previously and is usual in superplasticity, grain growth occurs during deformation within the gauge length [43], and justifies the observed n_{ap} values higher than 2.

Although n_{ap} values close to 3 have been obtained, solute drag (SD) dislocation glide mechanism [19,44] cannot be operative because of the following reasons. i) The as-received sample was subjected to an overaging treatment, being free of elements in solid solution prior to the ECAP processing; furthermore, at 300ºC, where the maximum elongation has been obtained, the presence of solid solution in this alloy by a possible dissolution of precipitates is negligible. ii) Solute drag mechanism controlled by dislocation glide is grain-size independent. Therefore, the stresses corresponding to the ECAP processed (with fine grain size) and the un-processed material (with coarse grain size) should be similar. However, at the test temperatures, the ECAP processed material is less creep resistant and presents much higher elongation than the as start material, until a mechanism change to dislocation creep due to grain coarsening is produced at 400ºC, presenting the two materials similar mechanical behaviour, as shown in Fig.3. iii) Strain rate change tests (SRC) have been performed, as shown in Fig.1, and no inverse transient creep has been observed. Under SD mechanism, upon an increase or decrease in strain rate, the flow stress undergoes a large, abrupt increase or decrease, and then gradually decays or increases toward a steady-state value until a new step in strain rate. Such inverse transients are exhibited only by SD creep in alloys with solid solution and, as such, can be used to positively identify the presence of this deformation mechanism [45,46]. Thus, the absence of transients in steps is consistent with deformation controlled by GBS creep. iv) High elongations are obtained under different tensile test conditions maintaining an equiaxed grain (Fig.4b and 5b). Under solute drag mechanism, highly elongated grains in the strain direction appear in the deformed

sample because this mechanism involves dislocation movement [26]. In addition, the consideration of the apparent stress exponent (n_{ap}) value as only evidence to determine the deformation mechanism may lead to an erroneous assessment of the operative mechanism. Thus, different experimental evidences, aside from n_{ap} and elongation values, must be verified to assign properly the operative deformation mechanism.

Thus, it is our contention that the different experimental evidences in the current work, such as dependence with grain size, equiaxed grains before and after deformation and random texture after deformation, apart from low stresses, high elongations and low stress exponent values, proof that grain boundary sliding is the operating mechanism, and thus the ECAPed alloy presents superplastic behavior in a window of testing conditions.

On the other hand, similar grain sizes are observed in the grip and gauge regions of the ECAPed sample at 300ºC (Fig. 5a and 5b) in contrast to the finer grain sizes observed in the gauge region in Fig. 4. This is attributed to the shorter time characterizing the test of Fig. 4. At the beginning of this test, the grain sizes are similar in the gauge and in the grip regions but the grains in the gauge region grew at a lower rate during the remaining time required for straining (about 2 min). This is attributed to the GBS mechanism, which is characterized by the elimination of dislocations through the grain boundaries, reducing the driving force for grain growth. However, the longer time during the SRC tests leads to similar grain growth in both regions.

In contrast to 300ºC, 350ºC is a critical temperature because non-homogeneous grain growth occurs, as observed clearly in the grip section (Fig. 5e). While the gauge section (Fig. 5f) shows fairly equiaxed grains with an average size of 3.8 ± 0.5 μm, a duplex microstructure is observed in the grip (Fig. 5e), with a small number of large grains being surrounded by fine grains, similar in size to those in the gauge section. The occurrence of a GBS mechanism under this test condition is corroborated by a n_{ap} value of ~3 (Fig. 3b) and the fairly equiaxed grain shape. Thus, while fine recrystallized grains are still retained in the gauge length during GBS straining (Fig. 5f), strong grain growth is taking place in the grip section during the whole time at test temperature (Fig. 5e), probably assisted by the beginning of precipitate dissolution at 350ºC. This precipitates dissolution should be also present in the gauge region. However, the decrease of driving force for grain growth associated with GBS should contribute to retain the equiaxed grain size observed in Fig. 5f.

Finally, large coarsening is observed after testing at 400ºC (Fig. 5g and h) in the gauge section and especially at the grip. The extensive precipitate dissolution that takes place above 350ºC explains this coarsening. The grains in the gauge length are elongated in the tensile direction due to a change between GBS at lower temperatures (250-300 ºC) and dislocation-dominated flow at 400ºC. This justifies the increase in

flow stress and in n_{ap} for the ECAPed sample at 400ºC observed in Fig. 3a and b respectively.

In summary, static recovery and continuous recrystallization taking place under some test conditions leads to microstructures prone to superplastic behaviour.

4. Conclusions

The Al 7075-T651 alloy has been subjected to overaging at 280ºC during 5h prior to ECAP processing and its mechanical properties at intermediate-high temperatures and the microstructure evolution have been analyzed. The main conclusions of this study are as follows:

1. The thermomechanical process performed allowed to obtain superplasticity at higher $\dot{\varepsilon}$ and lower temperature than those reported up to date for this alloy.
2. Although the as-processed sample showed a microstructure a priori little prone to superplastic behaviour, the occurrence of continuous recrystallization during heating at 300ºC previous to deformation, led to excellent ductility.
3. Despite this continuous recrystallization, the large grain refinement obtained during ECAP processing (~160 nm, f_{HAB}=56%) together with overaged pinning precipitates allowed the attainment of fine recrystallized grain size, 0.5-2 μm depending on the test conditions.
4. GBS is the dominant rate-controlling flow mechanism under test conditions of maximum ductility at 300ºC. This conclusion is supported by the presence of equiaxed grains, a grain size dependence and texture randomization in the gauge length of the tested samples. The solute drag dislocation glide mechanism has been dismissed, therefore, by experimental evidences.
5. At 350ºC, fine recrystallized grains were retained in the gauge length, while strong grain growth was observed in the grip section. This is attributed to the fact that GBS mechanism during straining reduces the driving force for grain growth.
6. The beginning of precipitate dissolution above 350ºC justifies the large grain coarsening observed after testing and the change of deformation mechanism to dislocation creep at high temperature.

Acknowledgements

Financial support from MICINN (Project MAT2009-14452) is gratefully acknowledged. Authors thank Professor Edgar Rauch from the Grenoble Institute of Technology (INPG), France, for experimental assistance with the ACOM-TEM technique.

References

1. F.C. Liu, Z.Y. Ma. Scripta Mater. 62 (2010) 125-128.

2. X. Liu, G. Du, R. Wu, Z. Niu, M. Zhang, J. Alloys Compd. 530 (2012) 48-55.

3. V.M. Segal. Mater. Sci. Eng. A 197 (1995) 157-164.

4. S. Ferrasse, V.M. Segal, K.T.H. Hartwig, R.E. Goforth. J. Mater. Res. 12 (1997) 1253-1261.

5. C-Y. Lin, H-J. Tsai, C-G. Chao, T-F. Liu, J. Alloys Compd. 530 (2012) 48-55.

6. P.B. Berbon, N.K. Tsenev, R.Z. Valiev, M. Furukawa, Z. Horita, M. Nemoto, T.G. Langdon. Metall. Mater. Trans. A 29 (1998) 2237-2243.

7. F.C. Liu, P. Xue, Z.Y. Ma, Mater. Sci. Eng. A 547 (2012) 55-63.

8. P. Málek, J. Erlebach, M. Cieslar, F.M. Knoop. Phys. Stat. Sol. A 157 (1996) 275-286.

9. M. Furukawa, Z. Horita, M. Nemoto, T.G. Langdon. Mater. Sci. Eng. A 297 (2001) 111-118.

10. Y. Deng, Z. Yin, K. Zhao, J. Duan, Z. He, J. Alloys Compd. 530 (2012) 71-80.

11. G. Shigesato, E.F. Rauch. Mater. Sci. Eng. A 462 (2007) 402-406.

12. E.F. Rauch, M. Veron. Materialwissenschaft und Werkstofftechnick. 36 (2005) 552-556.

13. E.F. Rauch, A. Duft. Mater. Sci. Forum. 495-497 (2005) 197-202.

14. F. Carreño, O.A. Ruano. Acta Mater. 46 (1998) 159-167.

15. C.M. Cepeda-Jiménez, J.M. García-Infanta, E.F. Rauch, J.J. Blandin, O.A. Ruano, F. Carreño, Metall. Mater. Trans. A (2012) *In Press.* DOI: 10.1007/s11661-012-1206-5.

16. G.R. Canova, U.F. Kocks, J.J. Jonas. Acta Metall. 32 (1984) 211-226.

17. A. Gholinia, P. Bate, P.B. Prangnell. Acta Mater. 50 (2002) 2121-2136.

18. P.K. Chaudhury, F.A. Mohamed, Acta Metall. 36 (1988) 1099-1110.

19. 17. O.D. Sherby, P.M. Burke. Progress Mater. Sci. 13 (1968) 323-390.

20. P. Metenier, G. González-Doncel, O.A. Ruano,J. Wolfenstine, O.D. Sherby, Mater. Sci. Eng. A 125 (1990) 195-202.

21. P. Acosta, J.A. Jiménez, G. Frommayer, O.A. Ruano, Mater. Letters 26 (1996) 97-101.

22. J.A. del Valle, O.A. Ruano, Acta Mater. 55 (2007) 455-466.

23. J.A. del Valle, F. Peñalba, O.A. Ruano, Mater. Sci. Eng. A 567 (2007) 165-171.

24. R.Z. Valiev, D.A. Salimonenko, N.K. Tsenev, P.B. Berbon, T.G. Langdon. Scripta Mater. 37 (1997) 1945-1950.

25. N. Tsuji, K. Shiotsuki, Y. Saito. Mater. Trans. 40 (1999) 765-771.

26. I. Charit, R.S. Mishra. J. Mater. Res. 19 (2004) 3329-3342.

27. P. Málek, P. Kratochvíl, J. Pesicka, P. Hanus, I. Sedivá. Intermetallics. 10 (2002) 985-992.

28. P. Lukác, K. Turba, P. Málek, M. Cieslar. Int. J. Mater. Res. (formerly Z Metallkd) 100 (2009) 847-850.

29. Glossary of Terms Used in Metallic Superplastic Materials, JIS H 7007, Japanese Standards Association, Tokyo, 1995, p.3

30. K. Higashi, M. Mabuchi, T.G. Langdon. ISIJ Intl. 36 (1996) 1423-1438.

31. P.B. Berbon, S. Komura, A. Utsunomiya, Z. Horita, M. Furukawa, M. Nemoto, T.G. Langdon. Mater. Trans. 40 (1999) 772-778.

32. K-T. Park, D-Y. Hwang, Y-K. Lee, Y-K. Kim, D-H. Shin. Mater. Sci. Eng. A 341 (2003) 273-281.

33. O.D. Sherby, R.H. Klundt, A.K. Miller. Metall. Trans. A 8 (1977) 843-850.

34. O.A. Ruano, O.D. Sherby. Revue Phys. Appl. 23 (1988) 625-637.

35. T.G. Nieh, L.M. Hsiung, J. Wadsworth, R. Kaibyshev. Acta Mater. 46 (1998) 2789-2800.

36. D.H. Bae, A.K. Ghosh. Acta Mater 50 (2002) 993-1009.

37. T.R. Mcnelley, K. Oh-Ishi, A.P. Zhilyaev, S. Swaminathan, P.E. Krajewski, E.M. Taleff. Metall. Mater. Trans. A 39 (2008) 50-64.

38. M.T. Pérez-Prado, T.R. McNelley, O.A. Ruano, G. González-Doncel. Metall. Mater. Trans. A 29 (1998) 485-492.

39. J.K. Mackenzie. Biometrika 45 (1958) 229-240.

40. J.A. del Valle, M.T. Pérez-Prado, O.A. Ruano. J. Eur. Ceram. Soc. 27 (2007) 3385-3390.

41. M.T. Pérez-Prado, T.R. McNelley, D.L. Swisher, G. Gonzalez-Doncel, O.A. Ruano. Mater. Sci. Eng. A 342 (2003) 216-230.

42. C.M. Hu, C.M. Lai, P.W. Kao, N.J. Ho, J.C. Huang. Mater. Charact. 61 (2010) 1043-1053.

43. S. Lee, P.B. Berbon, M. Furukawa, Z. Horita, M. Nemoto, N.K. Tsenev, R.Z. Valiev, T.G. Langdon. Mater. Sci. Eng. A 272 (1999) 63-72.

44. J. Weertman, J. Appl. Phys. 28 (1957) 1185-1189.

45. E.M. Taleff, W.P. Green, M.A. Kulas, T.R. McNelley, P.E. Krajewski. Mater. Sci. Eng. A 410-411 (2005) 32-37.

46. M.A. Kulas, W.P. Green, E.M. Taleff, P.E. Krajewski, T.R. McNelley. Metal. Mater. Trans. A 36 (2005) 1249-1261.

Figure Captions

Fig.1 Stress-strain curve obtained from a strain-rate-change test.

Fig.2 a) TEM micrograph, and b) orientation map and {111} pole figure obtained by ACOM-TEM of the ECAPed Al 7075-O alloy; c) boundary misorientation angle distribution (2-60º) of adjacent grains. Solid line in c) represents Mackenzie distribution.

Fig.3 Mechanical properties of the as-start and ECAPed Al 7075-O samples; a) strain rate-stress ($\dot{\varepsilon}$-σ) curves at various temperatures (200-400ºC), and b) variation of the apparent stress exponent (n_{ap}) versus strain rate ($\dot{\varepsilon}$) obtained from SRC tests; c) elongation to failure (e_F) against $\dot{\varepsilon}$ from tensile tests carried out at constant strain rate.

Fig.4 TEM micrographs of the a) grip region and b) and c) gauge deformed region of ECAPed Al 7075-O samples tensile tested at 300ºC and $\dot{\varepsilon}=10^{-2}$ s^{-1}.

Fig.5 EBSD maps and {111} pole figures of the a), e) and g) grip regions and b), f) and h) gauge deformed regions of ECAPed Al 7075-O samples tensile tested by SRC tests at 300, 350 and 400ºC; c) and d) show boundary misorientation angle distribution (2-60ºC) corresponding to EBSD maps in a) and b) respectively. The tensile direction is indicated by a horizontal arrow in b).

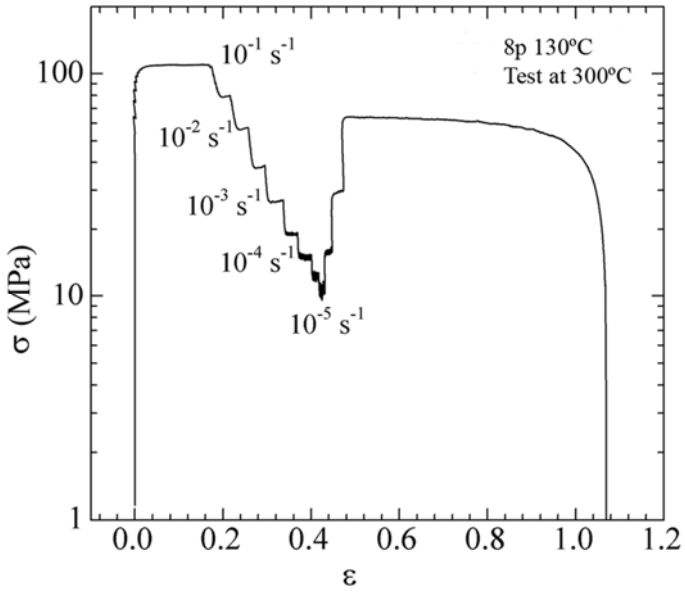

Fig.1 Stress-strain curve obtained from a strain-rate-change test.

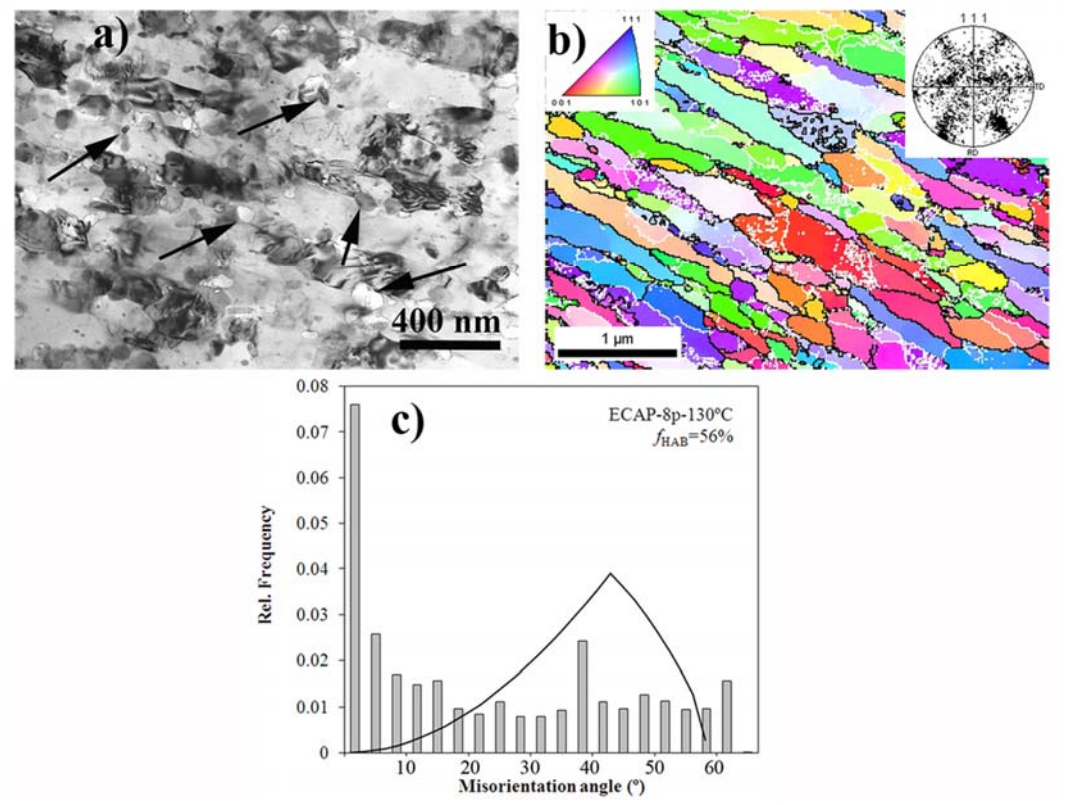

Fig.2 a) TEM micrograph, and b) orientation map and {111} pole figure obtained by ACOM-TEM of the ECAPed Al 7075-O alloy; c) boundary misorientation angle distribution (2-60º) of adjacent grains. Solid line in c) represents Mackenzie distribution.

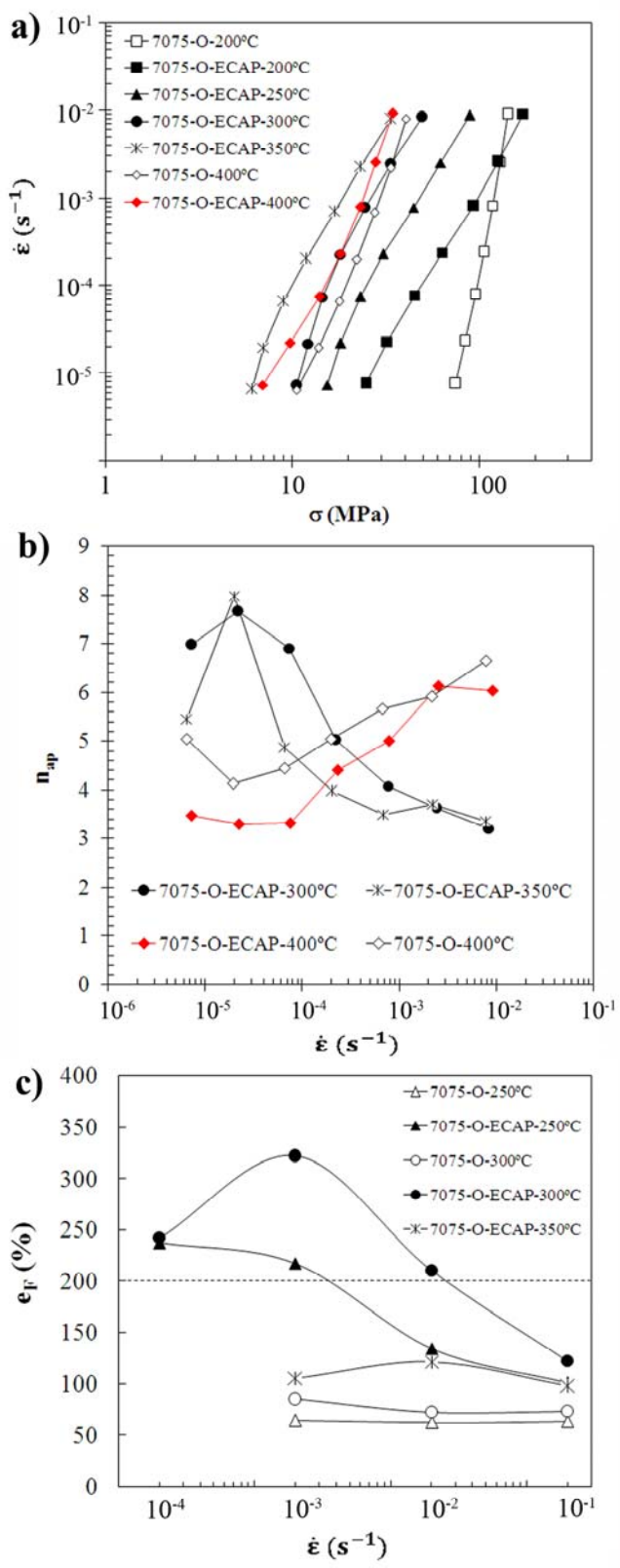

Fig.3 Mechanical properties of the as-start and ECAPed Al 7075-O samples; a) strain rate-stress ($\dot{\varepsilon}$-σ) curves at various temperatures (200-400ºC), and b) variation of the apparent stress exponent (n_{ap}) versus strain rate ($\dot{\varepsilon}$) obtained from SRC tests; c) elongation to failure (e_F) against $\dot{\varepsilon}$ from tensile tests carried out at constant strain rate.

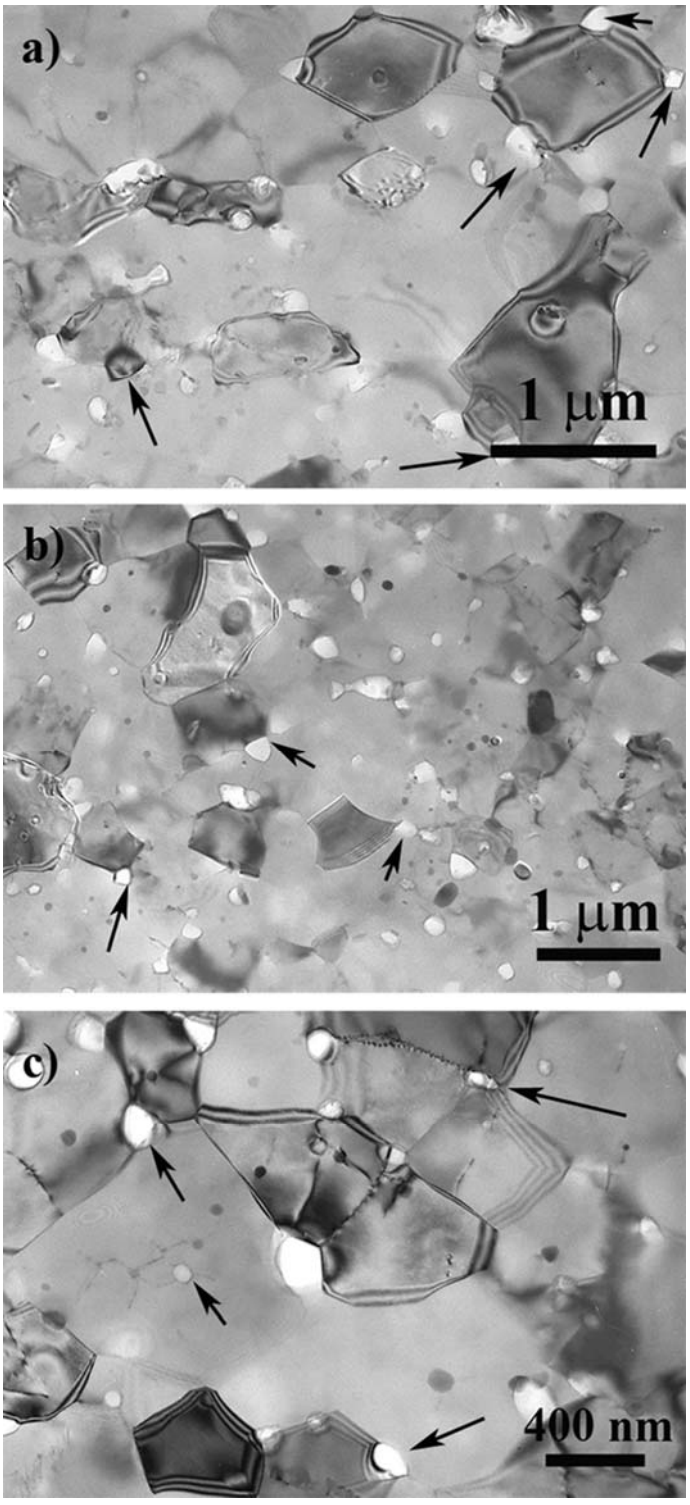

Fig.4 TEM micrographs of the a) grip region and b) and c) gauge deformed region of ECAPed Al 7075-O samples tensile tested at 300ºC and $\dot{\varepsilon}=10^{-2}$ s^{-1}.

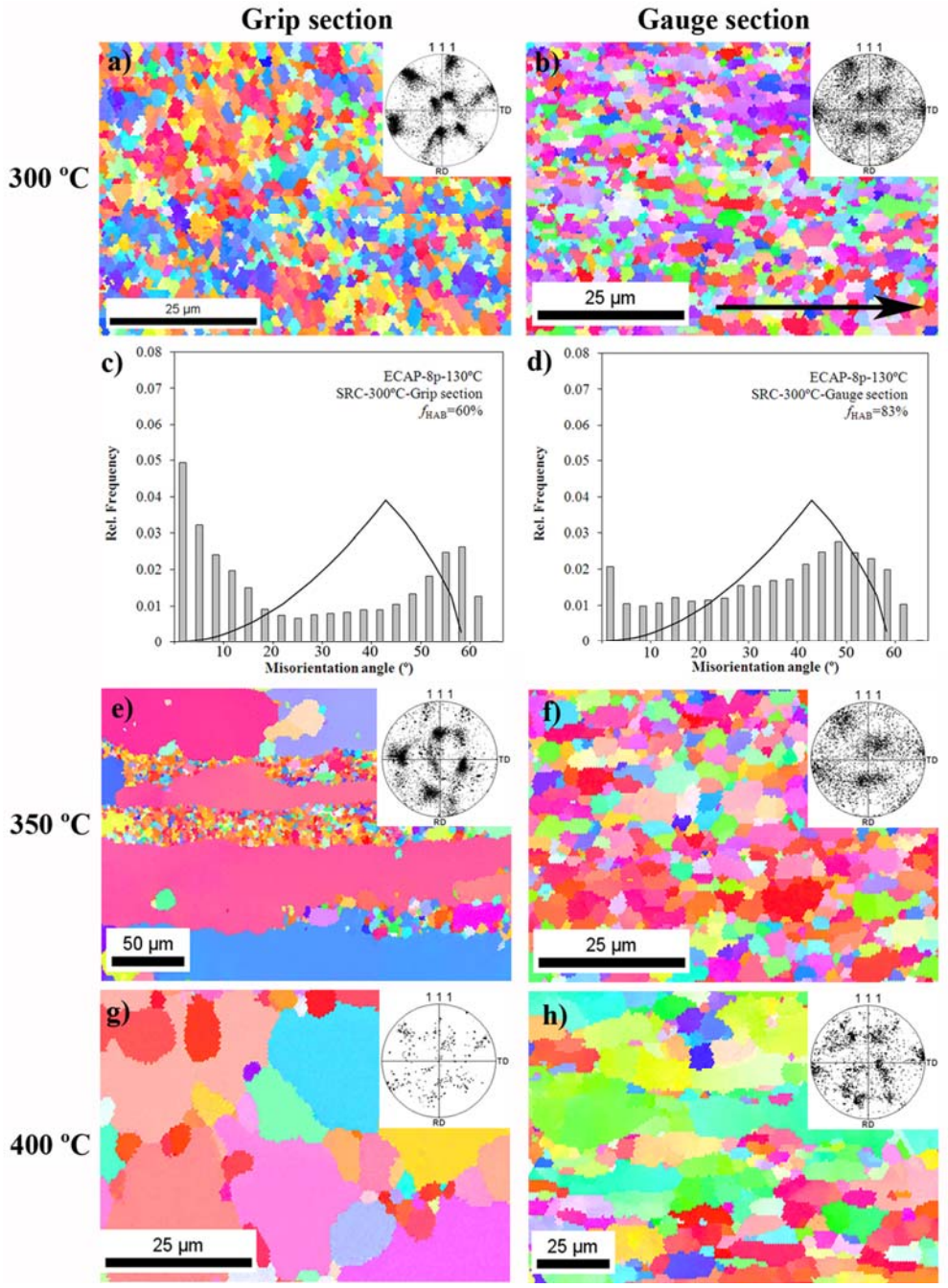

Fig.5 EBSD maps and {111} pole figures of the a), e) and g) grip regions and b), f) and h) gauge deformed regions of ECAPed Al 7075-O samples tensile tested by SRC tests at 300, 350 and 400ºC; c) and d) show boundary misorientation angle distribution (2-60ºC) corresponding to EBSD maps in a) and b) respectively. The tensile direction is indicated by a horizontal arrow in b).